## Electronic materials

# Enhancement of nonlinear optical property of Cu$_2$O/Ag/Cu$_2$O composite films induced by laser irradiation

Tingting Liu[1], Qingyou Liu[2], Yikai Jiang[1], Guohao Xia[1], Ruijin Hong[1,*] , Chunxian Tao[1], Qi Wang[1], Hui Lin[1], Zhaoxia Han[1], and Dawei Zhang[1]

[1] *Engineering Research Center of Optical Instrument and System, Ministry of Education and Shanghai Key Lab of Modern Optical System, University of Shanghai for Science and Technology, No.516 Jungong Road, Shanghai 200093, China*

[2] *Key Laboratory of High-Temperature and High-Pressure Study of the Earth's Interior, Institute of Geochemistry, Chinese Academy of Sciences, Guiyang 550081, China*

## ABSTRACT

In this paper, Cu$_2$O/Ag/Cu$_2$O nanocomposite films were obtained by controlling thermal oxidation Cu/Ag/Cu alloy films and then modified by laser irradiation under ambient condition. The effects of laser irradiation on the surface morphology, structure, optical properties and nonlinear performance of the sample were investigated. Those results indicate that the improvement of crystal quality, enhancement of Ag plasma peak and a large number of oxygen vacancy defects could be induced by laser irradiation. A switch from saturated absorption to reverse saturated absorption was observed in all samples with the excitation energy increasing. Compared with either single-layer or bilayer sample, the third-order nonlinear coefficient ($\beta$) of the sandwich structure samples was increased by 3.73 times after laser irradiation. In addition, the improvement of nonlinear performance of as-irradiated samples was also confirmed by finite difference time domain (FDTD) simulation results.

⚫ Springer

## GRAPHICAL ABSTRACT
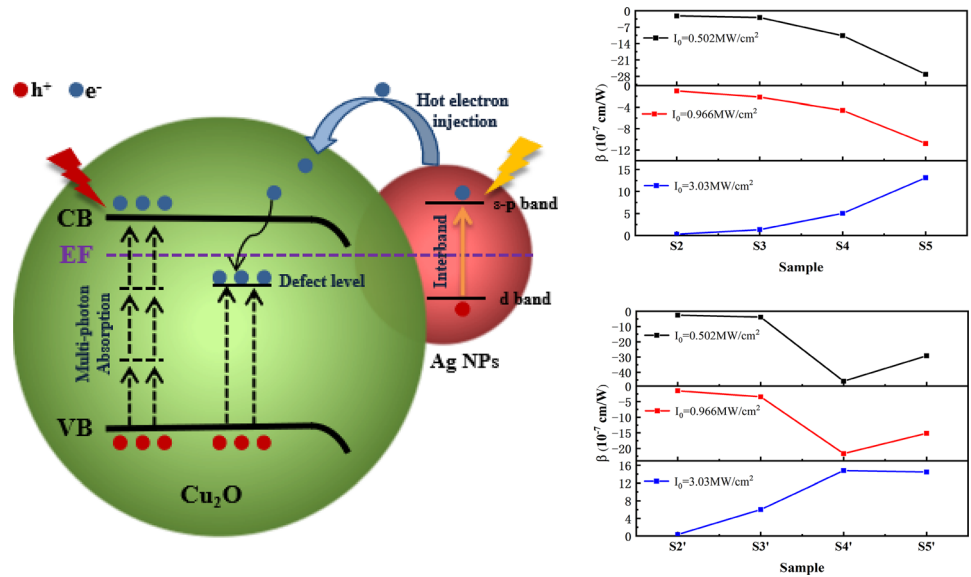


## Introduction

With the emergence of ultrashort pulse lasers and the gradual development of laser technology, people are increasingly studying nonlinear optics. Nonlinear optical effects play a very important role in modern photonics functional devices and systems, such as laser spectrum conversion, ultra-fast pulse generation, optical switching, all-optical modulation, etc. are all based on various nonlinear optical effects of materials [1–3]. Saturated absorption (SA) and reverse saturated absorption (RSA) are two contradictory reactions of the third-order nonlinear effects of materials, which have been reported in different nanomaterials [4–7]. SA is usually caused by the bleaching of the plasma ground state of the substance and is mainly used in optical switching and laser pulse compression. Free carrier absorption and multi-photon absorption are the main reasons for RSA. RSA can be used as an optical limiter that protects eyes and sensors from being damaged by sudden exposure to strong light [6]. Saturated absorption and reverse saturated absorption compete with each other. Therefore, we observe the conversion behavior from SA to RSA as the laser power increases in many metal–semiconductor composite structures [8–11].

Traditional nonlinear research started with inorganic materials (such as KDP and $LiNbO_3$), and then inorganic semiconductors such as GaAs and ZnS were used to control the nonlinear optical response of materials due to their adjustable band gap. In recent years, in order to meet the demand for more new optoelectronic components and devices, people are interested in new nonlinear materials (organic and inorganic materials). As a typical P-type semiconductor material, $Cu_2O$ has a band gap of about 2.17 eV and is widely used in solar cells [12], photocatalysis [13], sensors [14], and photodetectors [15]. Cuprous oxide has a center-symmetric cubic crystal structure and does not have a second-order nonlinear polarizability. Therefore, experimental research on the nonlinear optical properties of cuprous oxide has not appeared until the last decade. In 2009, Mani SE et al. [16] tested the third-order nonlinear polarizability of a single crystal cuprous oxide block for the first time. Sekhar et al. [6] found that the prepared $Cu_2O$ nanoclusters and microparticles all exhibit saturated absorption and reverse saturated absorption in 2012. Recently, Nabil A. Saad et al. [17] have prepared Ag-$Cu_2O$ nano-heterojunctions by co-

precipitation method, which confirmed that Ag nanoparticles (NPs) can enhance the linear and nonlinear performance of heterojunctions. Moreover, some Ag:$Cu_2O$ nanocomposite films with different silver content prepared on MgO substrates have been reported again. The results show that Ag NPs are embedded in $Cu_2O$, and the composite film has good electrical and optical properties [18, 19]. However, the nonlinear performance of samples with this sandwich structure is rarely reported.

In this paper, single-layer $Cu_2O$ film, bilayer Ag/$Cu_2O$ film and $Cu_2O$/Ag/$Cu_2O$ nanocomposite films with sandwich structure were fabricated by simple electron beam evaporation followed by thermal oxidation process. Furthermore, $CO_2$ laser irradiation, an economical and effective technology, was proposed to study its influence on the linear and nonlinear optical properties of samples. Then we studied the nonlinear absorption response of the sandwich structure samples using the Z-scan technique with an excitation wavelength of 1550 nm. The nonlinear response of the $Cu_2O$/Ag/$Cu_2O$ nanocomposite films was observed to transfer from saturated absorption to reverse saturated absorption with the increase of the excitation intensity. The enhancement of the nonlinear optical performance was observed in all as-irradiated samples.

## Experimental

Prior to deposition, borosilicate (BK7) glass substrates were cleaned in acetone, ethanol and deionized water for 15 min in turn using an ultrasonic cleaning machine, respectively. Metallic (Cu and Ag) thin films were deposited in turn on the substrates to form a sandwich structure by electron beam evaporation at room temperature. The thicknesses of the bottom and top layer for Cu thin film were both 20 nm. The middle layer of Ag thin film was controlled at 2, 7 and 12 nm, respectively. The thickness of the film was monitored by an in situ quartz crystal microbalance. The as-deposited Cu and Ag/Cu thin films were also fabricated for comparison. After deposition process, the as-deposited Cu film, Ag/Cu film and Cu/Ag/Cu composite films with increased Ag thicknesses were placed in a homemade tubular furnace and annealed under the ambient condition. The annealing temperature was maintained at 200 °C for 2 h. After the temperature of the tubular furnace

naturally reduced to room temperature, these as-annealed samples were taken out and marked as sample 1 (S1), sample 2 (S2), sample 3 (S3), sample 4 (S4) and sample 5 (S5), respectively. Due to annealing, the Cu film was oxidized to cuprous oxide along with the Ag thin films being transformed into nanoparticle structure. The structure schematic of these samples is shown in Fig. 1. Afterwards, laser irradiation by a continuous wave $CO_2$ laser source with the wavelength of 10.6 μm was applied to these films. The laser parameters of beam power, scanning rate and the beam diameter were set as 4 W, 50 mm/s and 0.1 mm, respectively. These as-irradiated samples were marked as sample 1′ (S1′), sample 2′ (S2′), sample 3′ (S3′), sample 4′ (S4′) and sample 5′ (S5′), respectively. To better understand, the specific parameters of all samples are shown in Table 1.

The crystal structure of the film was characterized by X-ray diffraction (XRD) using a Bruker AXS/D8 Advance system, with Cu Ka radiation ($\lambda = 0.15408$ nm). The surface morphology of the samples was characterized by atomic force microscope (AFM)(XE-100, Park System) with a 5 × 5 μm scanning area and scanning electron microscope (SEM)(S-4800, Hitachi), and surface roughness changes of the film sample were also reflected as well. Thermo Scientific K-Alpha$^+$ was used to study on the XPS. The UV–VIS–NIR double-beam spectrophotometer (Lambda1050, PerkinElmer, USA) was used to measure the optical absorption spectrum of samples, with the scanning range of 250–1200 nm and a
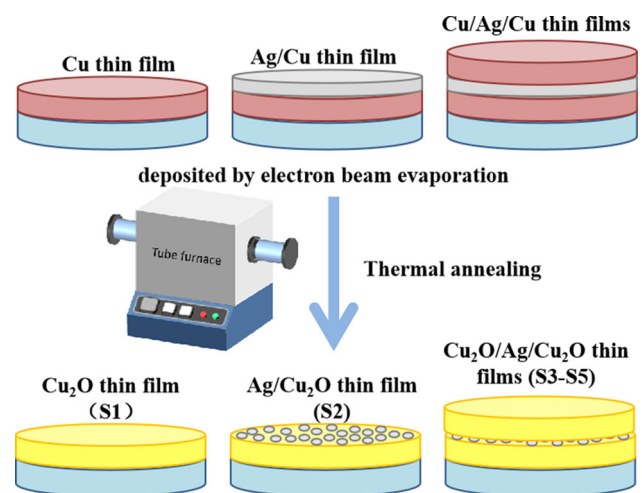


**Figure 1** Schematic of as-deposited Cu, Ag/Cu and Cu/Ag/Cu composite thin film structures and as-annealed $Cu_2O$, Ag/$Cu_2O$ and $Cu_2O$/Ag/$Cu_2O$ film samples structures.

**Table 1** Sample parameters

| Parameters | S1(S1′) | S2(S2′) | S3(S3′) | S4(S4′) | S5(S5′) |
|---|---|---|---|---|---|
| Structure | $Cu_2O$ | $Ag/Cu_2O$ | $Cu_2O/Ag/Cu_2O$ | $Cu_2O/Ag/Cu_2O$ | $Cu_2O/Ag/Cu_2O$ |
| Thickness (nm) | 20 | 2/20 | 20/2/20 | 20/7/20 | 20/12/20 |
| Annealing condition | 200 °C 2 h | | | | |

step length of 2 nm. The single-beam Z-scan technique based on optical distortion (self-focusing) was employed to measure the third-order nonlinear absorption coefficient. We used a mode-locked picosecond laser with a wavelength of 1550 nm, a duration of 2 ps and a repetition rate of 100 MHz as the optical excitation source which is focused through a 15-mm lens. All measurements were performed at room temperature.

# Results and discussion

## Microstructural properties and structural morphologies

Figure 2a–f shows the typical AFM images of samples before and after irradiation. According to Fig. 2a–c, the root mean square (RMS) surface roughness of the single-layer $Cu_2O$ (S1), bilayer $Ag/Cu_2O$ film (S2) and $Cu_2O/Ag/Cu_2O$ film in sandwich structure (S3) are 3.279, 2.578 and 3.707 nm, respectively. According to the result of AFM, the cover layer of Ag thin film has the effect of smoothing the surface of Cu2O thin film [17]. In the case of laser irradiation, the Ag NPs in as-annealed samples aggregated and grew on the $Cu_2O$ surface increasing the surface roughness [20], as shown in Fig. 2d–f, which also
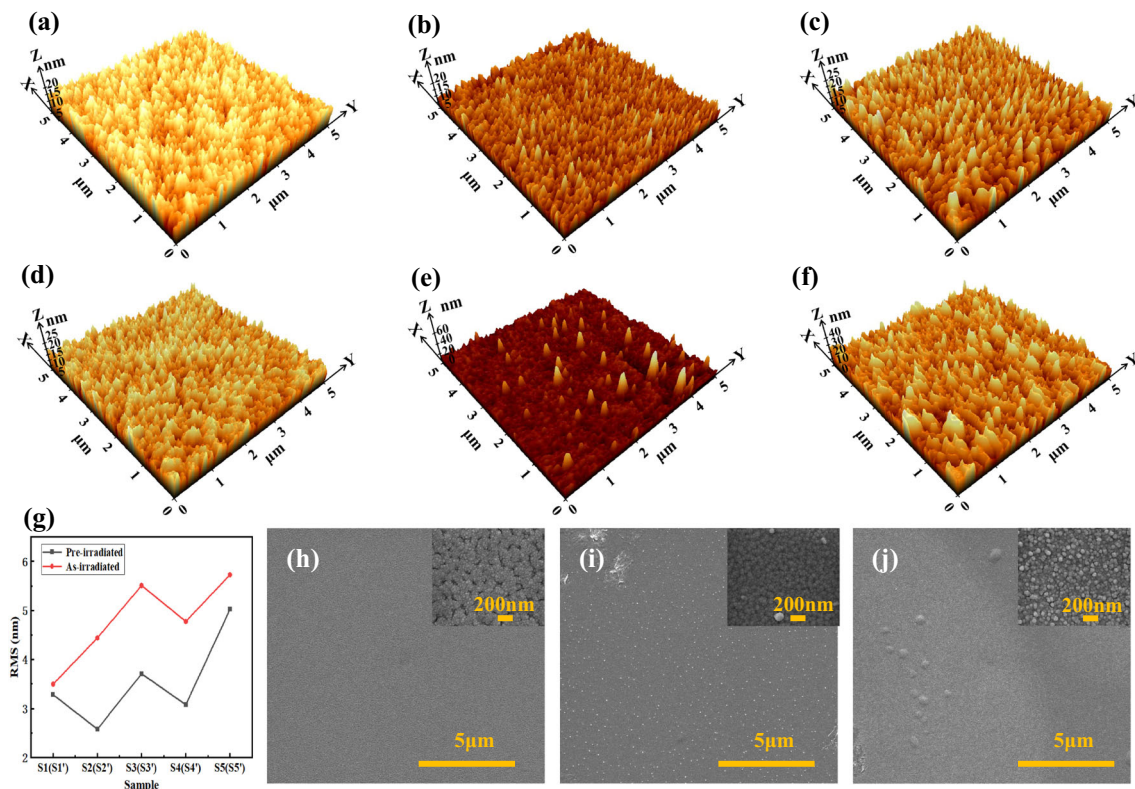


**Figure 2** AFM 3D images of **a** S1, **b** S2, **c** S3, **d** S1′, **e** S2′ and **f** S3′; **g** The surface roughness changes of samples before and after irradiation; SEM images of **h** S1′, **i** S2′ and **j** S3'.

corresponds to the absorption curve in Fig. 4. Figure 2g reveals the variation of surface roughness of all samples. In particular, the surface morphologies of the three-layer samples (S3–S5) are similar in AFM images, and the roughness increases with the increase in Ag layer thickness. The RMS surface roughness values of as-irradiated samples increased to 3.495, 4.438, 5.507, 4.775 and 5.726 nm, respectively. Figure 2h–j shows the representative SEM images of as-irradiated samples. As-irradiated pure cuprous oxide film was dense and uniform, and no obvious change in morphology was observed. After annealing at 200 °C, the Ag layer in the multilayer films was transformed into Ag particles [21]. Laser irradiation made the Ag particles larger, with a size of about 50–100 nm, as shown in Fig. 2i. Similarly, according to Fig. 2j, the aggregation of Ag particles resulted in a pore-like structure on the surface of the sandwich structure sample. Figure S1 of the supplementary material shows the particle diameter distribution histogram of the SEM images and their respective Gaussian fit. The mean particle diameter in S1′, S2′ and S3′ was determined to be 25.41, 37.57 and 52.25 nm, respectively. The increasing trend is consistent with the surface roughness of AFM images in Fig. 2g. Both the AFM and SEM images confirm that laser irradiation could change the Ag particle size resulting in the increase in surface roughness.

The XRD patterns of all samples are shown in Fig. 3 to reveal the influence of laser irradiation on crystal structures of films. No obvious diffraction peaks are observed in both $Cu_2O$ and $Ag/Cu_2O$ samples, because that they are amorphous phase with thin thickness. However, two diffraction peaks at 36.56°(2θ) and 37.96°(2θ) can be observed in the $Cu_2O/Ag/Cu_2O$ samples both before and after irradiation, which correspond to the (111) peak of $Cu_2O$ phase (JCPDS No. 56–3288) and the (111) plane of Ag phase (JCPDS No. 89–3722), respectively. According to Fig. 3a, the diffraction peak intensity of $Cu_2O$ in the three-layer composite films increased with the increase in the silver thickness. The main reason is that both thermal annealing and the increase in the metal contact Ag layer thickness lead to the metal-induced solid-phase crystallization effect of the cuprous oxide film [22, 23]. After laser irradiation, $Cu_2O$ and Ag diffraction peaks are also slightly enhanced, as shown in Fig. 3b. It is attributed to the recrystallization of the crystal grains caused by the thermal action of the laser irradiation [24]. These results show that laser irradiation-induced $Cu_2O$ and Ag particles to crystallize to the (111) surface with the lowest surface energy, which improved the crystallinity of the films.

## Optical characterization

The absorption spectra of the samples are shown in Fig. 4, which mainly reflects the influence of laser irradiation on the absorption characteristics of $Cu_2O$, $Ag/Cu_2O$ and $Cu_2O/Ag/Cu_2O$ samples. The as-annealed single-layer $Cu_2O$ film shows an absorption peak near 348 nm, which is caused by scattering and interband transitions in $Cu_2O$ [25]. Meanwhile, the overall absorption intensity improved in the visible and near-infrared regions in the $Ag/Cu_2O$ nanocomposite film, as shown in Fig. 4a. The change
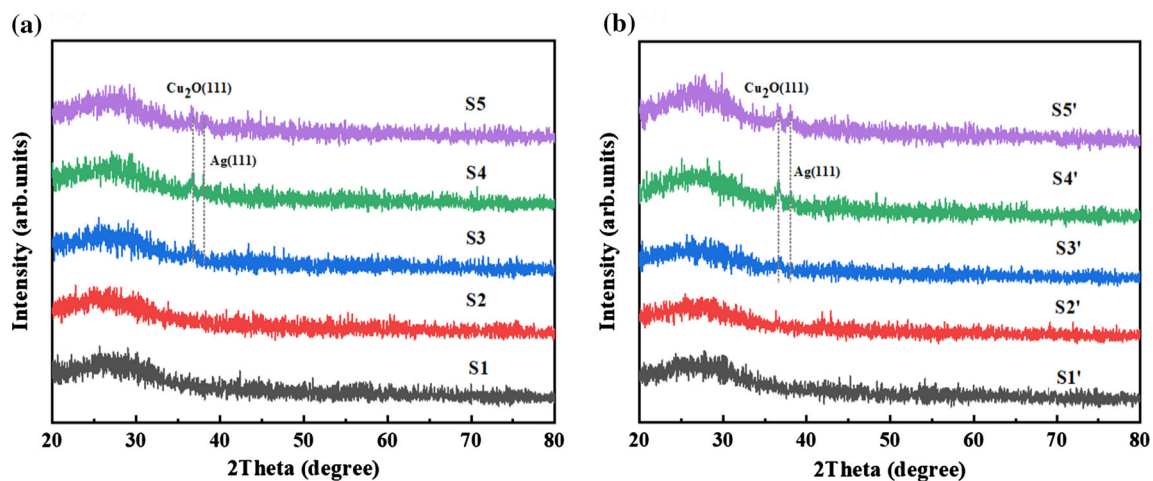


**Figure 3** XRD patterns of **a** as-annealed samples (S1-S5) and **b** as-irradiated samples (S1′–S5′).
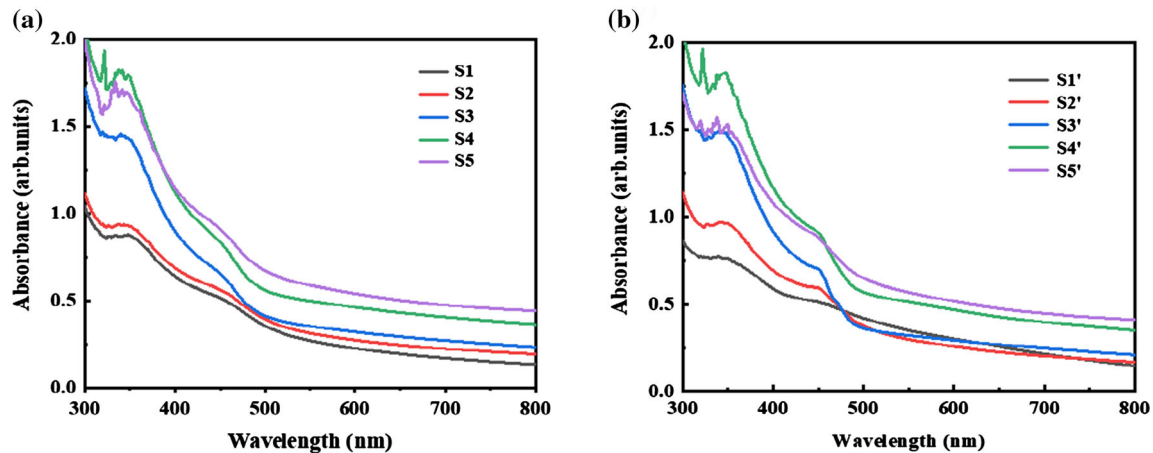
**Figure 4** Absorption spectra of **a** as-annealed samples (S1-S5) and **b** as-irradiated samples (S1′–S5′).

in this range is due to the combined effect of the plasmonic effect of Ag NPs and the absorption or reflection caused by the embedded Ag NPs in the $Cu_2O$ lattice [19]. In addition, for $Cu_2O/Ag/Cu_2O$ samples, the absorption peak of $Cu_2O$ (348 nm) firstly strengthened and then weakened with the increase in Ag thickness. The reason for this trend is that with the increase in the Ag middle layer thickness, the Ag layer transfers into continuous Ag nanofilm, affecting the absorption of cuprous oxide in the lower layer [26]. Figure 4b shows the absorption curves of all samples irradiated by the laser. After laser irradiation, pure $Cu_2O$ surface was slightly oxidized and weakened the $Cu_2O$ peak intensity, resulting in the absorption in the visible region of 400–800 nm. However, a new absorption peak near 450 nm was observed in the as-irradiated $Ag/Cu_2O$ film, which corresponds to the plasmon resonance peak of Ag NPs [27]. According to the SEM images, it is demonstrated that the Ag NPs on the surface aggregated by laser irradiation, which enables the existence of stronger LSPR [28]. For the three-layer samples (S3′–S5′) after irradiation, the samples with thinner Ag layer (2 and 7 nm) mainly showed the absorption peak of Ag near 450 nm and had a small redshift (from 450 to 456 nm), but the absorption peak of Ag for the film with thicker Ag layer (12 nm) exhibits little effect. Therefore, when a multilayer sample with an appropriate Ag thickness (7 nm) was irradiated by the laser, the grains further grew to aggregated Ag NPs and finally enhanced plasmon resonance of Ag and the coupling between $Cu_2O$ and Ag was used to improve the absorption characteristics of $Cu_2O/Ag /Cu_2O$ multilayer films.

The Tauc function toward the estimation of band gap energy of all samples is plotted and displayed in Fig. S2. The band gap energy of pure $Cu_2O$ is 2.37 eV, which is similar to that reported in the literature [6]. The absorption edge shifted toward longer wavelength with the introduction of Ag layer [19]. The band gap of as-irradiated $Cu_2O$ is reduced owing to surface oxidation. However, the aggregation of Ag NPs in as-irradiated $Ag/Cu_2O$ film increases its optical band gap. For the as-irradiated three-layer samples (S3′–S5′), laser irradiation shows slight effect.

## Composition and valence state

X-ray photoelectron spectroscopy (XPS) measurement is applied to analyze the influence of irradiation on the composition and chemical state of the sandwich structure sample (S4), and to reflect the interaction between $Cu_2O$ and Ag by comparing the Ag XPS peak drift of $Ag/Cu_2O$ bilayer film (S2) and S4. Figure 5a shows the XPS measurement spectrum of S4, which confirms the presences of Cu, O, and Ag elements in the hybrid samples. The XPS spectra of Cu 2p in S1, S1′, S4 and S4′ are shown in Fig. 5b–c. Two peaks at 932.1–932.8 eV and 952.0–952.8 eV correspond to the Cu $2p_{3/2}$ and Cu $2p_{1/2}$ peaks of $Cu^+$, respectively. At the same time, the Cu $2p_{3/2}$ and Cu $2p_{1/2}$ peaks of $Cu^{2+}$ correspond to the characteristic bands between 933.7–934.3 eV and 954.2–954.4 eV, respectively [29–32]. It confirms that the surface of the film is oxidized to CuO in the case of annealing [33]. The content of $Cu^+$ in the as-irradiated samples increased, because of the formation of a solid layer on the surface of $Cu_2O$ film delays
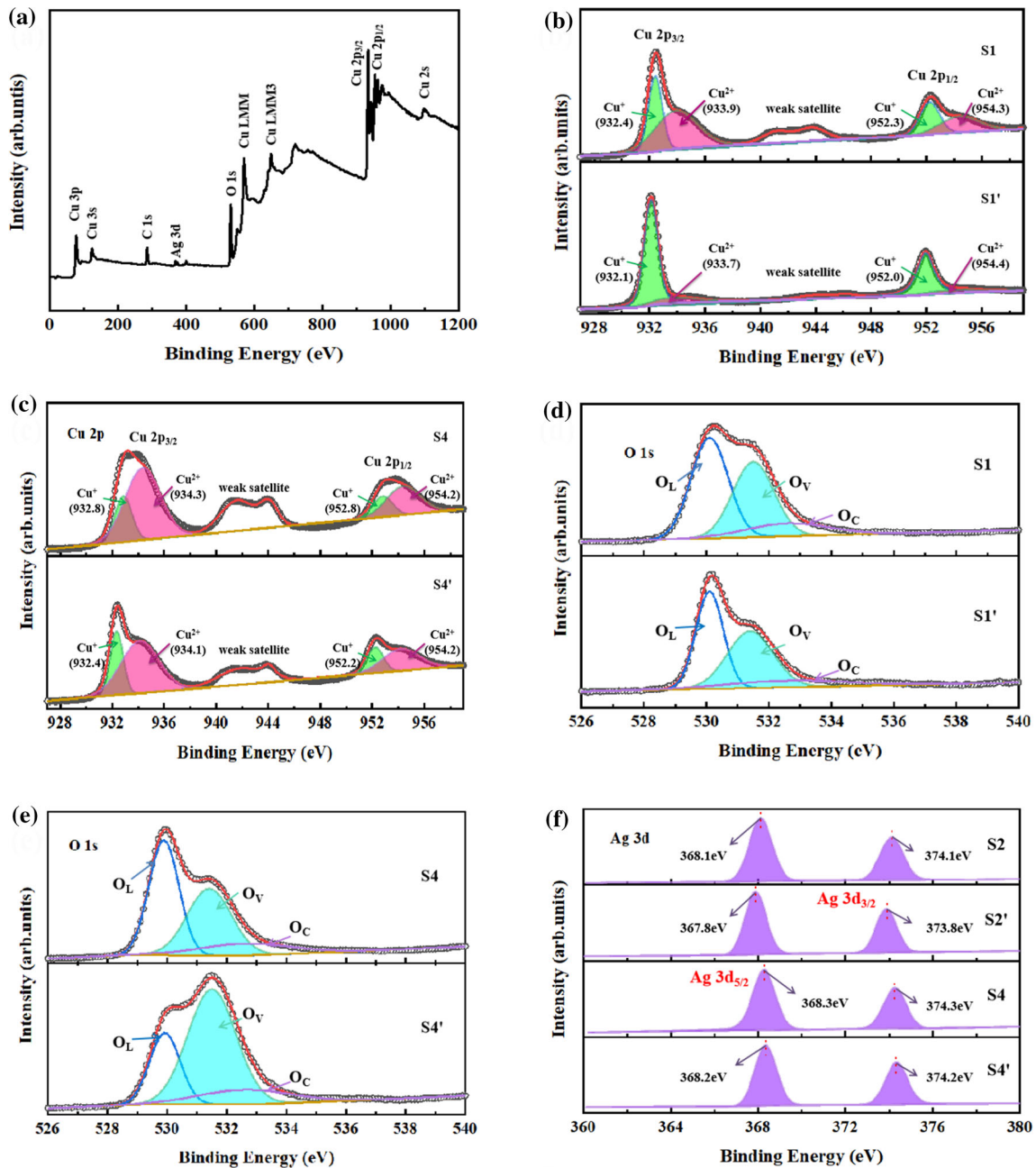
**Figure 5** **a** XPS survey spectrum of S4; XPS spectra of Cu 2p for **b** S1 and S1′, **c** S4 and S4′; O1s for **d** S1 and S1′, **e** S4 and S4′ and Ag 3d for **f** S2, S2′, S4 and S4′.

oxidation. The O 1 s spectra of S1, S1′, S4 and S4′ are exhibited in Fig. 5d–e, which can be divided into three peaks. The observed peak at 530 eV is assigned to lattice oxygen atoms in $Cu_2O$ ($O_L$), and the binding energy at 531.4 eV is attributed to oxygen vacancy ($O_V$). Further, the peak at 532.6 eV is corresponding to chemisorbed oxygen ($O_C$) or hydroxyl ions [29, 34]. The $O_V$ peak area of pure $Cu_2O$ film only increased by 3% after laser irradiation. The relative percentage

of peak areas for $O_V$ is 38.5% for S4, whereas the percentage is 60.5% for S4′. It indicates that S4′ has more oxygen vacancies than S4, which is caused by the introduction of defects and the formation of mesoporous structures due to the thermal action of the $CO_2$ continuous laser irradiation process. It is possible that the abundant oxygen vacancy in as-irradiated three-layer samples could account for the enhanced third-order nonlinear performance of as-

irradiated three-layer samples compared with other samples [19]. In addition, Fig. 5f further compares the Ag 3d XPS spectra of S2, S2′, S4 and S4′. It is obvious that the peak binding energies of Ag $3d_{5/2}$ and Ag $3d_{3/2}$ in S4 are 368.3 eV and 374.3 eV, respectively [21, 35, 36]. The orbital splitting energy of 3d doublet is about 6 eV which further evidences the metallic state of Ag-matrix. By comparing S2 and S4, we found that the binding energy of Ag in the sandwich structure samples was slightly higher, which may be caused by the increase in the thickness of Ag [37]. Moreover, it is known that the binding energy of the irradiated sample Ag shifts to a lower energy direction compared by the samples before and after the irradiation (S2 and S2′, S4 and S4′). It may be caused by the effect of laser irradiation on the interaction between $Cu_2O$ and Ag of the sample.

## Nonlinear optical properties

Figure 6 reveals the normalized transmittance of the multilayer samples before and after laser irradiation measured by the open aperture Z-scan system with different excitation powers, and the excitation wavelength is 1550 nm. The total nonlinear absorption coefficient of the sample can be described as: $\alpha = \alpha_0 + \beta I$, where $I$, $\alpha_0$ and $\beta$, respectively, represent excitation light intensity, the linear absorption coefficient and nonlinear absorption coefficient [38]. So the propagation equation of the sample can be expressed as: $\frac{dI}{dz} = -\alpha_0 I - \beta I^2$. For the open aperture Z-scan, the normalized transmittance $T_{Norm}$ is given as:

$$T_{Norm} = 1 - \frac{1}{2\sqrt{2}}\frac{\beta I_0 L_{eff}}{1 + \left(\frac{z}{z_0}\right)^2} \tag{1}$$

Here, $L_{eff} = [1 - e^{-\alpha_0 L}]/\alpha_0$ is the effective optical length, $z$ represents the straight-line distance between the sample and the focal point, and $z_0$ represents the diffraction length of the beam. Additionally, $I_0$ is the laser intensity focused at $z = 0$ through the lens, and $L$ is the thickness of the film sample [39].

Regardless of the increase in excitation power or the influence of laser irradiation, the $Cu_2O$ and Ag/ $Cu_2O$ samples have no obvious nonlinear absorption phenomenon. The nonlinear curve trends of the two are similar, so only the normalized transmittance curve of the Ag/$Cu_2O$ bilayer film is shown in Fig. 6. According to Fig. 6a–b, when the sample is excited by

the excitation light with a peak irradiance of 0.502 MW/cm$^2$, the three-layer film (S3–S5) exhibits saturated absorption behavior, and the peak value of the sample increases with the increase in Ag thickness. What's more, the nonlinear performance of all samples has been enhanced after laser irradiation. Among them, S4′ reaches the maximum value, which is consistent with the absorption curve. But when the peak excitation intensity increases to 0.966 and 3.03 MW/cm$^2$, the sandwich structure sample will change from saturated absorption to reverse saturated absorption. This indicates that the increase in excitation intensity will lead to a decrease in saturated absorption and an increase in reverse saturated absorption. As indicated in Fig. 6g–h, $\beta$ value of S4′ changes from $-45.75 \times 10^{-7}$ to $14.79 \times 10^{-7}$ cm/W with the enhancement of excitation energy, while, at the maximum excitation intensity, laser irradiation makes the $\beta$ value of sample S4 increase from $-10.66 \times 10^{-7}$ to S4′ of $-45.75 \times 10^{-7}$ cm/W. It is indicated that laser irradiation can effectively improve the nonlinear performance of the samples. In addition, we compare the current working $\beta_{eff}$ value with the test value reported in the previous literature in Table 2 Comparison of the nonlinear absorption coefficient $\beta$eff values of this work with those reported in the literature. This tells that $Cu_2O$/ Ag/$Cu_2O$ nanofilms exhibit a higher $\beta_{eff}$ value, which is mainly due to the influence of laser irradiation and unique sandwich structure.

Many different mechanisms which lead to the switch from saturated absorption to reverse saturated absorption have been reported [10, 17, 40, 41]. This study proposes a possible mechanism for enhancing the nonlinear performance of the $Cu_2O$-Ag nanocomposite structure as shown in Fig. 7a. Here, the SA effect is mainly attributed to the plasma ground state bleaching effect caused by the interband transition from d orbit to s–p orbit in Ag NPs or a small amount of energy level transition in $Cu_2O$. The RSA effect is caused by five-photon absorption in Ag, free-carrier absorption or multi-photon absorption in $Cu_2O$. At lower intensity, the saturated absorption of the sample dominates, and the excitation intensity reaches a certain value. Also, the reverse saturated absorption exceeds the saturated absorption to reverse the response of the sample. On the one hand, the nonlinear absorption of $Cu_2O$ and Ag samples (S2–S5) coupled with each other, which is caused by the superposition of multiple absorption
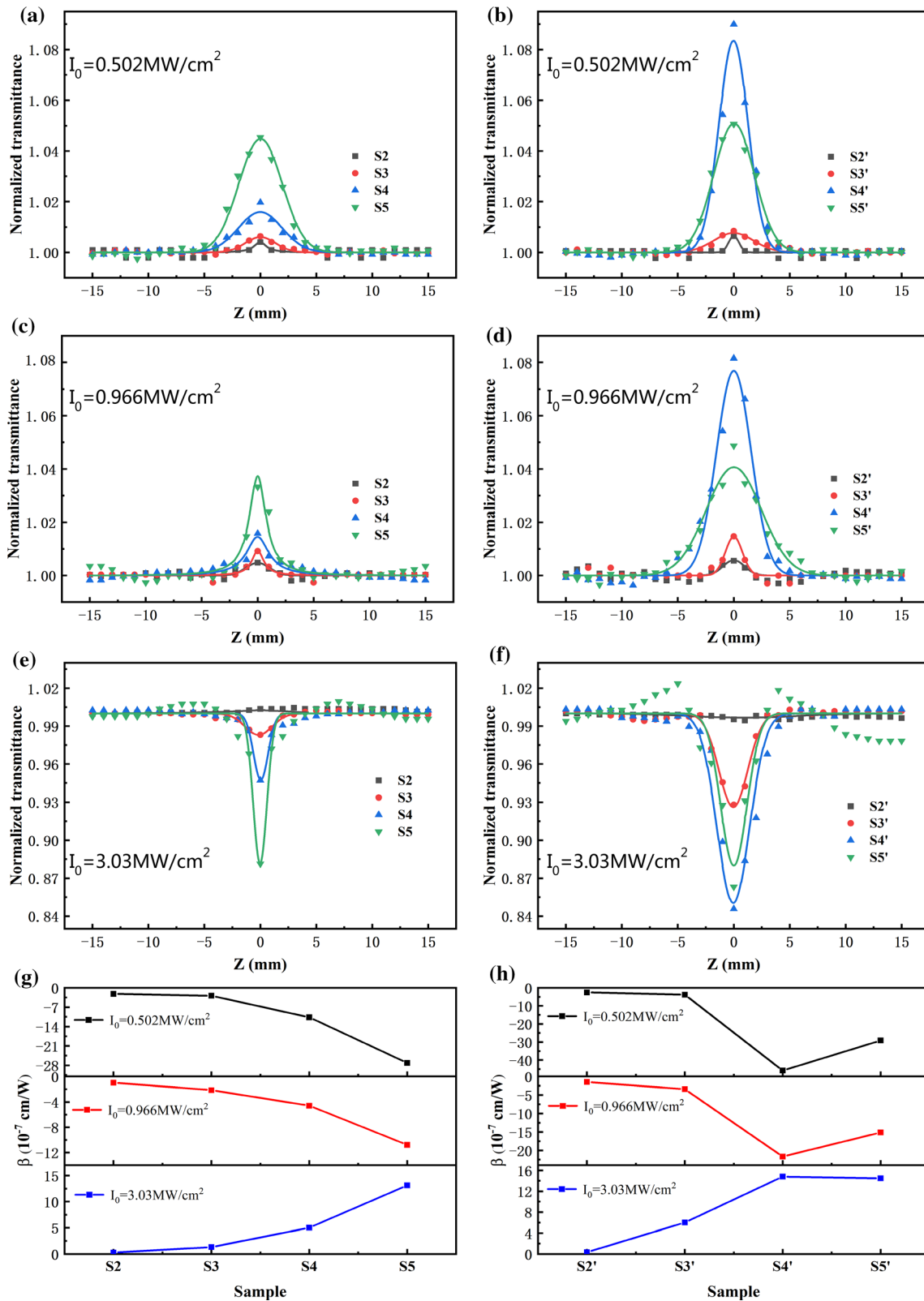
**Figure 6 a–f** Open aperture Z-scan curves of as-annealed samples (S2–S5) and as-irradiated samples (S2′-S5′); **g-h** The values of nonlinear absorption (*β*) of the samples.

**Table 2** Comparison of the nonlinear absorption coefficient $\beta_{eff}$ values of this work with those reported in the literature

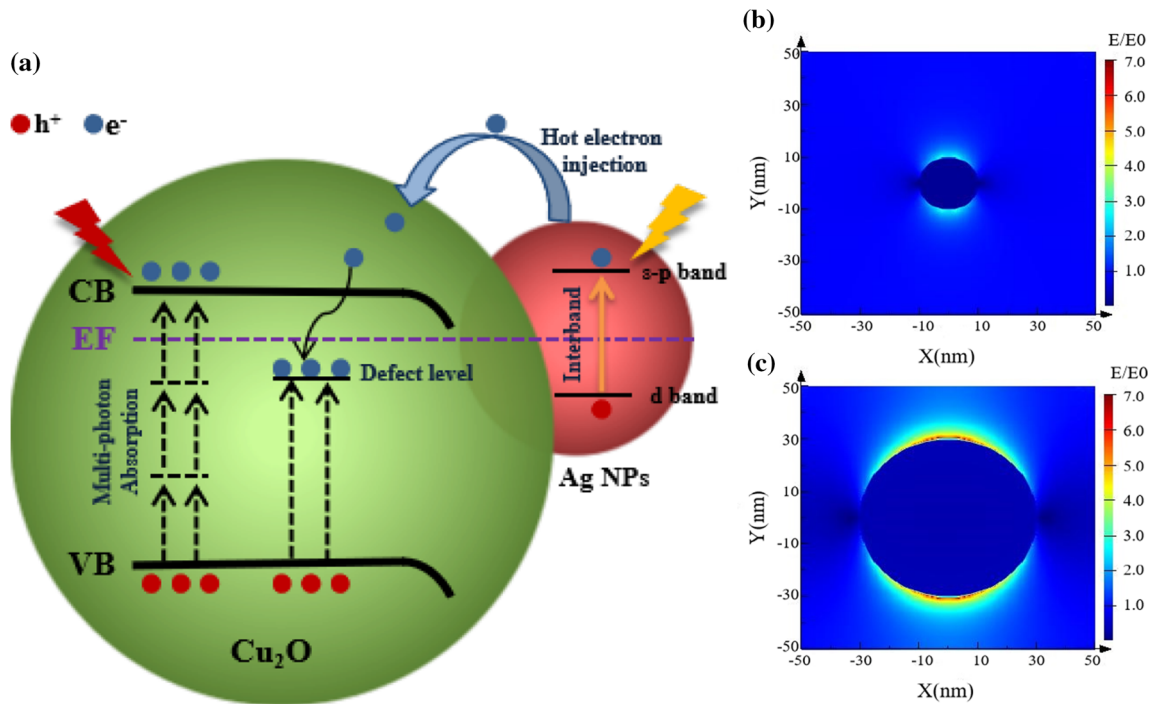| Sample material | Wavelength (nm) | $\beta_{eff}$ (cm/W) | References |
|---|---|---|---|
| $Cu_2O$ thin film | 800 | $4 \times 10^{-8}$ | Fu et al. [42] |
| $Cu_2O$ NPs | 532 | $1.9 \times 10^{-8}$ | Sekhar et al. [6] |
| Au@$Cu_2O$ NRs | 580–818 | $1.22 \times 10^{-9}$ | Gong et al. [43] |
| $Cu_2O$ –Ag NPs | 1064 | $2.6 \times 10^{-7}$ | Saad et al. [17] |
| AgCu/$Al_2O_3$ nanofilm | 400 | $4.5 \times 10^{-7}$ | Gao et al. [44] |
| $Cu_2O$/Ag/$Cu_2O$ nanofilm | 1550 | $45.75 \times 10^{-7}$ | Current work |



**Figure 7** **a** The nonlinear mechanism for $Cu_2O$ thin films decorated with Ag NPs; The FDTD simulated electric field amplitude patterns of **b** as-annealed and **c** as-irradiation $Cu_2O$/Ag/$Cu_2O$ thin films.

effects, compared with pure $Cu_2O$ samples (S1). On the other hand, laser irradiation could introduce a large number of oxygen vacancy defects and can form defect energy levels between the conduction band and valence band of cuprous oxide. As shown in Fig. 7a, electrons are more likely to transition from the conduction band to the defect energy level, accelerating the charge transfer rate. As an excellent conductor, Ag NPs can effectively separate the electron–hole pairs generated by $Cu_2O$. At the same time, laser irradiation enhances the interaction between $Cu_2O$ and Ag NPs, and the increase in electron mobility can explain the enhancement of the nonlinear performance of the sample.

In order to further study the influence of laser irradiation on the electric field distribution of hybrid samples, we simulated the electric field distribution

of $Cu_2O$/Ag/$Cu_2O$ thin film before and after irradiation excited by excitation light with a wavelength of 1550 nm using finite difference time domain (FDTD) method, as shown in Fig. 7b–c. The smaller size of Ag NPs in the $Cu_2O$/Ag/$Cu_2O$ film is formed by annealing, and the electric field intensity was 2.84. Ag NPs aggregated after laser irradiation, and the electric field intensity of the three-layer sample increased to 7.02. It can be attributed to the strong coupling, which is caused by the increase in the size of Ag NPs and the increase in the contact area between $Cu_2O$ and Ag particles. The FDTD results well show that laser irradiation can enhance the local electric field of the sample, thereby improving the nonlinear performance of the sample.

## Conclusion

In summary, we studied the effects of laser irradiation on $Cu_2O/Ag/Cu_2O$ multilayer films. Those measurement results show that the laser irradiation has the effect of aggregating Ag NPs inducing the formation of mesoporous structure, improving the optical band gap and crystallinity of the multilayer film, and introducing oxygen vacancy defects in the samples. According to nonlinear absorption (NLA) results, both saturated absorption and reverse saturated absorption behaviors could be observed in all samples. In addition, it is demonstrated that the enhancement of nonlinear absorption in as-irradiated samples is attributed to the carrier migration accelerated by defect energy level and the strong coupling between $Cu_2O$ and Ag.

## Acknowledgements

## References

[1] Kauranen M, Zayats AV (2012) Nonlinear plasmonics. Nat Photonics 6:737–748

[2] Chen HJ, Shao L, Li Q, Wang JF (2013) Gold nanorods and their plasmonic properties. Chem Soc Rev 42:2679–2724

[3] Hartland GV (2011) Optical studies of dynamics in noble metal nanostructures. Chem Rev 111:3858–3887

[4] Dini D, Calvete MJF, Hanack M (2016) Nonlinear optical materials for the smart filtering of optical radiation. Chem Rev 116:13043–13233

[5] Cesca T, Calvelli P, Battaglin G, Mazzoldi P, Mattei G (2012) Local-field enhancement effect on the nonlinear optical response of gold-silver nanoplanets. Opt Express 20:4537–4547

[6] Sekhar H, Narayana Rao D (2012) Preparation, characterization and nonlinear absorption studies of cuprous oxide nanoclusters, micro-cubes and micro-particles. J Nanopart Res. https://doi.org/10.1007/s11051-012-0976-4

[7] Fu M, Wang K, Long H, Yang G et al (2012) Resonantly enhanced optical nonlinearity in hybrid semiconductor quantum dot: metal nanoparticle structures. Appl Phys Lett. https://doi.org/10.1063/1.3683548

[8] Elim HI, Yang J, Lee JY, Mi J et al (2006) Observation of saturable and reverse-saturable absorption at longitudinal surface plasmon resonance in gold nanorods. Appl Phys Lett. https://doi.org/10.1063/1.2177366

[9] Gao YC, Zhang XR, Li YL, Liu HF, Wang YX et al (2005) Saturable absorption and reverse saturable absorption in platinum nanoparticles. Opt Commun 251:429–433

[10] Wang S, Zhang Y, Zhang R, Yu H, Zhang H, Xiong Q (2015) High-order nonlinearity of surface plasmon resonance in Au nanoparticles: paradoxical combination of saturable and reverse-saturable absorption. Adv Opt Mater 3:1342–1348

[11] Tian X, Wei R, Yang D, Yang D, Qiu J et al (2020) Paradoxical combination of saturable absorption and reverse-saturable absorption in plasmon semiconductor nanocrystals. Nanoscale Adv 2:1676–1684

[12] McShane CM, Choi K-S (2012) Junction studies on electrochemically fabricated p-n $Cu2O$ homojunction solar cells for efficiency enhancement. Phys Chem Chem 14:6112–6118

[13] Huang L, Peng F, Yu H, Wang HJ (2009) Preparation of cuprous oxides with different sizes and their behaviors of adsorption, visible-light driven photocatalysis and photo-corrosion. Solid State Sci 11:129–138

[14] Cui G, Zhang P, Chen L, Wang X et al (2017) Highly sensitive H2S sensors based on $Cu2O/Co3O4$ nano/microstructure heteroarrays at and below room temperature. Sci Rep-UK. https://doi.org/10.1038/srep43887

[15] Wang J, Yang J, Yang J, Zhang H et al (2020) CNT/$Cu2O$ heterojunction via self-assembly technology for emerging flexible photodetectors. J Mater Sci-Mat 31:5892–5899. https://doi.org/10.1007/s10854-019-02818-4

[16] Mani SE, Jang JI, Ketterson JB (2009) Large third-order susceptibility and third-harmonic generation in centrosymmetric $Cu2O$ crystal. Opt Lett 34:2817–2819

[17] Saad NA, Dar MH, Ramya E, Naraharisetty RG, Rao DN (2019) Saturable and reverse saturable absorption of a $Cu2O$-Ag nanoheterostructure. J Mater Sci 54:188–199. https://doi.org/10.1007/s10853-018-2811-5

[18] Meng G, Wang XM, Hu H, Zhao H et al (2019) $Cu2O$-Ag nanocomposites with tunable optical property. Mater Res Expre. https://doi.org/10.1088/2053-1591/ab3cb5

[19] Yin HB, Zhao Y, Li J, Yang Q, Wu WD (2020) Optical and electrical properties of Ag:$Cu2O$ nanocomposite films prepared by pulse laser deposition. Mater Chem Phys. https://doi.org/10.1016/j.matchemphys.2019.122399

[20] Hong RJ, Sun WF, Liu QY, Li ZW et al (2019) Al-induced tunable surface plasmon resonance of Ag thin film by laser

irradiation. Appl Phys Expre. https://doi.org/10.7567/1882-0786/ab2c30

[21] Wei Q, Wang Y, Qin HY, Wu JM, Lu YF et al (2018) Construction of rGO wrapping octahedral Ag-Cu2O heterostructure for enhanced visible light photocatalytic activity. Appl Catal B-En 227:132–144

[22] Yang C, Hirose Y, Nakao S et al (2012) Metal-induced solid-phase crystallization of amorphous TiO2 thin films. Appl Phys Lett. https://doi.org/10.1063/1.4739934

[23] Garcia-Serrano J, Gomez-Hernandez E, Ocampo-Fernandez M, Pal U (2009) Effect of Ag doping on the crystallization and phase transition of TiO2 nanoparticles. Curr Appl Phys 9:1097–1105

[24] Wang TJ, Wang DM, Zhang H, Wang XL, Chen M (2017) Laser-induced convenient synthesis of porous Cu2O@CuO nanocomposites with excellent adsorption of methyl blue solution. Opt Mater Expre 7:924–931

[25] Li JT, Cushing SK, Bright J, Meng FK et al (2013) Ag@Cu2O core-shell nanoparticles as visible-light plasmonic photocatalysts. Acs Catal 3:47–51

[26] Li H, Li X, Wang W, Huang J, Li J et al (2019) Ultraflexible and biodegradable perovskite solar cells utilizing ultrathin cellophane paper substrates and TiO2/Ag/TiO2 transparent electrodes. Sol Energy 188:158–163

[27] Yang ZQ, Ma CC, Wang W, Zhang MT et al (2019) Fabrication of Cu2O-Ag nanocomposites with enhanced durability and bactericidal activity. J Colloid Inter 557:156–167

[28] Hong RJ, Shao W, Sun WF et al (2018) Laser irradiation induced tunable localized surface plasmon resonance of silver thin film. Opt Mater 77:198–203

[29] Zhang YH, Cai XL, Guo DY, Zhang HJ et al (2019) Oxygen vacancies in concave cubes Cu2O-reduced graphene oxide heterojunction with enhanced photocatalytic H-2 production. J Mater Sci-Mat 30:7182–7193

[30] Zhang QY, Huang LH, Kang SF, Yin CC et al (2017) CuO/Cu2O nanowire arrays grafted by reduced graphene oxide: synthesis, characterization, and application in photocatalytic reduction of CO2. Rsc Adv 7:43642–43647

[31] Zheng Q, Wei Y, Zeng XH, Xia WW et al (2020) Effect of bandgap alignment on the photoreduction of CO(2)into methane based on Cu2O-decorated CuO microspheres. Nanotechnology. https://doi.org/10.1088/1361-6528/ab9f74

[32] Wang Z, Liang X, Zhu Y, Zouhu X, Feng X, Zhu R (2019) Ag and Cu2O modified 3D flower-like ZnO nanocomposites and evaluated by photocatalysis oxidation activity regulation. Ceram Int 45:23310–23319

[33] Chen YC, Chen YJ, Popescu R, Dong PH et al (2019) Defect-cluster-boosted solar photoelectrochemical water splitting by n-Cu2O thin films prepared through anisotropic crystal growth. Chemsuschem 12:4859–4865

[34] Wan CC, Jiao Y, Li J et al (2017) Multilayer core-shell structured composite paper electrode consisting of copper, cuprous oxide and graphite assembled on cellulose fibers for asymmetric supercapacitors. J Power Sources 361:122–132

[35] Yang KX, Yan ZG, Ma L, Du YP et al (2019) A facile one-step synthesis of cuprous oxide/silver nanocomposites as efficient electrode-modifying materials for nonenzyme hydrogen peroxide sensor. Nanomaterials-B. https://doi.org/10.3390/nano9040523

[36] Lin XF, Zhou RM, Zhang JQ, Fei ST (2009) A novel one-step electron beam irradiation method for synthesis of Ag/Cu2O nanocomposites. Appl Surf Sci 256:889–893

[37] Li JX, Xu JH, Dai WL, Fan KN (2009) Dependence of Ag deposition methods on the photocatalytic activity and surface state of TiO2 with Twistlike Helix structure. J Phys Chem C 113:8343–8349

[38] Li ZW, Hong RJ, Liu QY, Wang Q et al (2020) Laser patterning induced the tunability of nonlinear optical property in silver thin films. Chem Phys Lett. https://doi.org/10.1016/j.cplett.2020.137535

[39] Serna J, Rueda E, Garcia H (2014) Nonlinear optical properties of bulk cuprous oxide using single beam Z-scan at 790 nm. Appl Phys Lett. https://doi.org/10.1063/1.4901734

[40] Wang Y, Wang Y, Chen K, Qi K et al (2020) Niobium carbide MXenes with broad-band nonlinear optical response and ultrafast carrier dynamics. ACS Nano 14:10492–10502

[41] Sakar M, Balakumar S (2018) Reverse Ostwald ripening process induced dispersion of Cu2O nanoparticles in silver-matrix and their interfacial mechanism mediated sunlight driven photocatalytic properties. J Photoch Photobiol A 356:150–158

[42] Fu M, Long H, Wang K, Yang G, Lu P (2011) Third order optical susceptibilities of the Cu2O thin film. Thin Solid Films 519:6557–6560

[43] Gong L, Qiu Y, Nan F, Hao Z, Zhou L, Wang Q (2018) Synthesis and largely enhanced nonlinear refraction of Au@Cu2O core-shell nanorods. Wuhan Univ J Nat Sci 23:418–423

[44] Gao X, Zou C, Zhou H, Yuan C et al (2020) Enhanced nonlinear optical properties of alloyed AgCu glassy nanoparticles. J Alloy Compd. https://doi.org/10.1016/j.jallcom.2019.153003

**Publisher's Note** Springer Nature remains neutral with regard to jurisdictional claims in published maps and institutional affiliations.